Initial observations of the femtosecond timing jitter at the European XFEL

Henry J. Kirkwood,[1] [iD] Romain Letrun,[1] [iD] Takanori Tanikawa,[1] Jia Liu,[1] Motoaki Nakatsutsumi,[1] Moritz Emons,[1] Tomasz Jezynski,[1] Guido Palmer,[1] Max Lederer,[1] Richard Bean,[1] Jens Buck,[2] Samuele Di Dio Cafisio,[1,3] Rita Graceffa,[1] Jan Grünert,[1] Sebastian Göde,[1] Hauke Höppner,[1,3] Yoonhee Kim,[1] Zuzana Konopkova,[1] Grant Mills,[4] Mikako Makita,[1] Alexander Pelka,[1,3] Thomas R. Preston,[1] Marcin Sikorski,[1] Cedric M. S. Takem,[1] Klaus Giewekemeyer,[1] Matthieu Chollet,[5] Patrik Vagovic,[1,6] Henry N. Chapman,[6] [iD] Adrian P. Mancuso,[1,4] and Tokushi Sato[1,6,*] [iD]

[1]European XFEL GmbH, Holzkoppel 4, Schenefeld, 22869, Germany
[2]Christian-Albrechts-Universität zu Kiel, Institut für Experimentelle und Angewandte Physik, Leibnizstrasse 19, Kiel 24098, Germany
[3]Institute for Radiation Physics, Helmholtz-Zentrum Dresden-Rossendorf, Bautzner Landstrasse 400, Dresden 01328, Germany
[4]Department of Chemistry and Physics, La Trobe Institute for Molecular Science, La Trobe University, Melbourne, VIC 3086, Australia
[5]Linac Coherent Light Source, SLAC National Accelerator Laboratory, 2575 Sand Hill Road, Menlo Park, California 94025, USA
[6]Center for Free-Electron Laser Science, Deutsches Elektronensynchrotron, Notkestrasse 85, Hamburg 22607, Germany
*Corresponding author: tokushi.sato@xfel.eu

Intense, ultrashort, and high-repetition-rate X-ray pulses, combined with a femtosecond optical laser, allow pump-probe experiments with fast data acquisition and femtosecond time resolution. However, the relative timing of the X-ray pulses and the optical laser pulses can be controlled only to a level of the intrinsic error of the instrument which, without characterization, limits the time resolution of experiments. This limitation inevitably calls for a precise determination of the relative arrival time, which can be used after measurement for sorting and tagging the experimental data to a much finer resolution than it can be controlled to. The observed root-mean-square timing jitter between the X-ray and the optical laser at the SPB/SFX instrument at European XFEL was 308 fs. This first measurement of timing jitter at the European XFEL provides an important step in realizing ultrafast experiments at this novel X-ray source. A method for determining the change in the complex refractive index of samples is also presented.

Ultrashort, ultrabright X-ray pulses provided by novel X-ray free electron laser (XFEL) facilities are enabling new studies in the chemical, physical, and biological sciences. The ultrabright pulses allow the study of weakly scattering objects such as single particles [1–3] and sub-micrometer sized crystals [4] free of radiation damage [5] from the nanometer down to the atomic scale. Very recently, megahertz data collection became feasible [6,7]. The ultrashort pulse duration also allows time-resolved experiments on the timescale of atomic motions [8,9], one of the primary motivations for XFELs. The time-resolved optical laser pump/X-ray probe technique is a well-established experimental method and is becoming a common tool for investigating ultrafast dynamics of protein molecules [10–14]. For this class of experiments, femtosecond timing accuracy over the whole period of data collection is crucial to their success. Current XFEL sources generate pulses with durations down to a few femtoseconds [15,16]. However, the shot-to-shot timing jitter of the pump-probe (PP) delay of a few tens to hundreds of femtoseconds can corrupt any benefit of using ultrashort pulse durations if this jitter is not correctly characterized for each pulse. At hard XFEL facilities, this timing jitter has been thoroughly investigated, the Linac Coherent Light Source reports timing jitter better than 118.9 fs root-mean-square (RMS) [280 fs in full width at half-maximum (FWHM)] [17], the SPring-8 Angstrom Compact Free Electron Laser (SACLA) measured a timing jitter of 256 fs RMS (603 fs FWHM) [18], and the X-ray free-electron laser at the Pohang Accelerator Laboratory reports timing jitter of 24.7 fs RMS (58.2 fs FWHM) [19]. The intrinsic timing jitter of the X-ray beam is mainly due to the nature of non-seeded self-amplified spontaneous emission (SASE) in the accelerator [20,21]. Accelerator sub-components and synchronization systems also contribute to the timing jitter and can introduce long-term drift [18,22]. Therefore, the major experimental challenge in achieving femtosecond timing resolution is to remove the effects of timing jitter over multiple timescales [23–25].

The most promising solution is the development of *in situ* methods to measure the relative delays [26–29] and "time tag" each pulse. This method is becoming a key part of time-resolved experiments and uses a "measure-and-sort" approach, where the

relative delay time of each pulse is measured and used to sort the data in time with demonstrated sub-femtosecond accuracy [30].

This Letter reports on the first measurement of the PP timing jitter of the SASE-1 branch of the European XFEL (EuXFEL) [31] using the spectral encoding method [26,32]. The results show a timing jitter of 308 fs RMS with uncertainties of 36 fs accuracy with the current RF synchronization system. We further demonstrate that the X-ray induced modulation in the complex refractive index of a material can be determined using a space-shifted implementation of spectral interferometry [33] by inserting a Mach–Zehnder interferometer (MZI) into the spectral encoding setup.

These measurements were conducted at the Single Particles, Clusters, and Biomolecules and Serial Femtosecond Crystallography (SPB/SFX) instrument [34], at the SASE-1 branch at the EuXFEL. The spectral encoding setup (Fig. 1) was mounted downstream of the primary SPB/SFX interaction region. The spectral encoding technique uses a linearly chirped optical laser pulse which spatially and temporally overlaps the XFEL pulse at the sample position. Different spectral components of the chirped optical pulse arrive at the sample at different times, providing a direct mapping of wavelength to time. The interaction of an X-ray pulse with the sample leads to a change of its optical properties, a sharp jump in the optical spectrum at the relative time of arrival. The XFEL beam was operated at a photon energy of 10.5 keV with a pulse energy of approximately 800 µJ and duration of 50 fs. The beam was focused by a stack of beryllium compound refractive lenses after passing through a 1 mm thick silicon attenuator. The sample for the spectral encoding was positioned downstream of the focus where the X-ray beam diameter was 200 µm. The 800 nm, 15 fs pulse provided by the EuXFEL central PP laser system [35] was chirped by a 200 mm Schwerflintglas 57 (SF57) rod to obtain a total time window of 12.7 ps in $1/e^2$ and wavelength envelope of 765–845 nm in FWHM. The diameter of the optical laser beam on the sample was 400 µm in FWHM and was nearly collinear with the X-ray beam. By using a probe with a larger footprint on the sample than that of the X-ray pump, the measurement is insensitive to the pointing jitter of the XFEL beam. The change in probe transmission through the sample was measured by a Shamrock 193i imaging spectrometer (Andor Technology Ltd.) with a 600 line/mm diffraction grating that was equipped with a 6.5 µm pixel, cooled sCMOS 16 bit camera (Photonic Science Ltd.). The spectrometer was measured to have a wavelength calibration of 0.043 nm per pixel corresponding to a pixel to time

mapping of 6.6 fs/pixel. The width of the camera sensor, 1920 pixels, yielded a total time window of approximately 13 ps. Throughout the experiment, the train rate of both the XFEL and the optical laser were set to 10 Hz with a single pulse per train. The PP laser seed oscillator was synchronized to the EuXFEL mode-locked master laser oscillator (MLO), which is again phase-locked to the RF Master Oscillator. The synchronization of the PP laser to the optical reference is based on a phase-locked loop type phase-detection scheme at the 25th harmonic (1354 MHz) of the oscillator repetition rate with a measured in-loop jitter of <30 fs RMS. Once combined with the all-optical two-color balanced optical cross-correlational scheme to precisely measure the timing error between the seed oscillator and the MLO, the relative timing jitter and drift will be reduced substantially with a goal of 10 fs RMS [36] in the near future.

Spectral interferometry is a well-known optical technique for retrieving the phase and amplitude of an unknown electric field in the femtosecond time domain [33]. An MZI was inserted into the spectral encoding path after the sample. The two arms of the MZI were shifted and tilted to obtain fringes in the spatial domain such that two different regions of the incident optical pulse were interfered, one region from the unperturbed part of the sample and one from the perturbed part. The resulting two-dimensional interferogram consists of one spatial dimension and one spectral dimension. As described by Geindre *et al.* [33], the spectral power (and, hence, the amplitude) is obtained along the spectral dimension and the probe phase from the spatial dimension. Hence, the change in the amplitude of the optical probe is still encoded in the spectral domain, as with the spectral encoding method, but now the change in phase is additionally encoded in the spatial domain by using the MZI. The spectral encoding method requires a reference measurement from the unperturbed sample to calculate the relative change in transmission; in contrast to using spectral interferometry, the change in phase is a single shot measurement, and no reference is required. Hence, the change in the sample's complex refractive index induced by each individual XFEL shot is observed as a modulation in both the amplitude and phase of the optical probe.

The sample was 10 µm thick $Gd_{2.8}La_{0.2}Fe_5O_{12}$ gadolinium iron garnet (GIG) on a $(GdCa)_3(GaMgZr)_5O_{12}$ gadolinium gallium garnet (GGG) substrate. The GIG sample has a large ($\approx 74\%$) X-ray absorption at the photon energy of 10.5 keV.

First, the spectral encoding method (without the MZI) was used to measure the PP timing jitter. The relative change in optical transmission, $\Delta T(t)$, of the sample, as a function of time, t, is defined as $\frac{S_{sig}(t)}{S_{ref}(t)} - 1$, where S_{sig} and S_{ref} are the transmitted spectral intensities at the X-ray pumped and unpumped areas, respectively. These one-dimensional spectra were obtained by summing across a region of 60 pixels through the center of the X-ray pumped region (with constant time, t). To account for shot-to-shot variation in optical pulse intensity and spectrum, large numbers of reference pulses were measured. The cross-correlation between each individual S_{sig} and S_{ref} was calculated from a region of the spectra that was unpumped by the X-ray beam. The transmission change, $\Delta T(t)$, was calculated using the reference signal S_{ref} which had the highest cross-correlation with a given S_{sig}. To determine the relative arrival time of each pulse, the change in sample transmission was modeled in terms of the maximum transmission change ΔT_{max}, the effective Gaussian
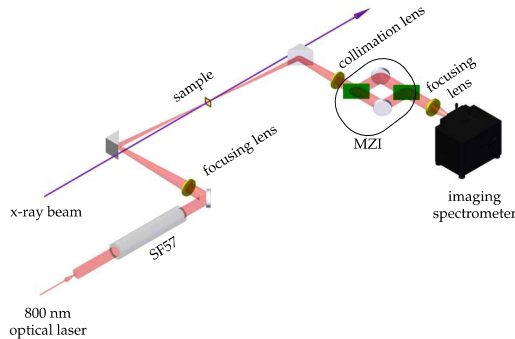

Fig. 1. Spectral encoding setup with the MZI. The optical laser pulse was chirped using 200 mm of Schwerflintglas 57 (SF57), and temporally and spatially overlapped with the X-ray pulse at the sample position.

pulse shape centered at time t_0 with width τ_1 and exponential decay of τ_2 [30]:

$$\Delta T(t) = \frac{\Delta T_{\max}}{2}\left[\mathrm{erf}\left(\frac{t-t_0}{\tau_1\sqrt{2}}\right)+1\right]\exp\left(-\frac{t-t_0}{\tau_2}\right), \quad \textbf{(1)}$$

where erf is the error function. The relative time of arrival, change in transmission, width, and decay were determined by the fitting equation (1) to the transmission change calculated for 2045 individual X-ray pulses. To eliminate abnormal shots in the pump or probe beams or misfits from the subsequent analysis, the pulses with a change in transmission of less than 10% were excluded. This resulted in a subset of 2028 individual pulses. Figure 2(a) shows an example of the measured reference and signal spectra. The relative transmission change is also shown with the corresponding model fit. After determining the relative arrival time (t_0) of each X-ray pulse with respect to the corresponding optical probe, the data were sorted by the relative delay, as shown in Fig. 2(b). The arrival-time jitter measured with the spectral encoding method was 308 fs in RMS (724 fs FWHM) with an uncertainty of 36 fs, calculated from the variance of the fit parameters. The change in transmission was relatively unaffected by pulse energy fluctuations of the incident X-ray beam, as shown in Fig. 2(c).

The MZI was then inserted into the optical path downstream of the sample, as shown in Fig. 1; the spatial fringes obtained can be seen in Fig. 3(b). The resulting two-dimensional interferogram consists of one spatial dimension [vertical in Fig. 3(b)] and one spectral dimension [horizontal in Fig. 3(b)]. The method to determine the relative change in transmission of the sample has been described above and follows the same process (in the spectral domain). The change in phase of the broadband spectrum was determined by taking the one-dimensional Fourier transform of the interferogram for each wavelength (i.e., of the spatial domain) and isolating one of the lateral peaks that lie around $\pm 2\pi/d$, where d is the unperturbed interfringe distance, then calculating the phase of this frequency component. The result is a vector of phase angles as a function of probe wavelength (time).

For the GIG sample, the phase (as a function of wavelength) shows similar behavior to the change in transmission where there is a large step-like change induced by the XFEL pulse. Figure 4 shows an example of the transmission and phase change for a single pulse, as well as the phase measured without X-rays.
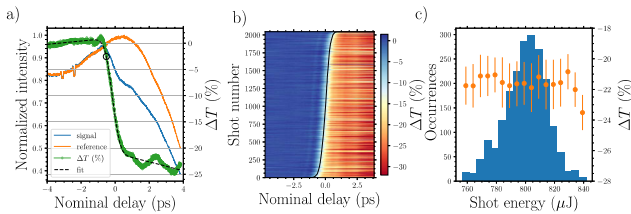

Fig. 3. (a) Single shot image from the spectral encoding which shows the amplitude only. (b) Image from the spectral encoding with MZI, which shows both the amplitude and phase shift (by fringes). In both images, the change induced by the XFEL pulse can be found at the nominal delay of 0 ps.

The phase measured without X-rays is approximately constant in this region of the optical spectrum. The same fitting procedure was applied to the phase shift and used to determine t_0. Figure 4 also shows the difference in t_0 as determined from the amplitude and phase. In all cases, t_0 is defined as the time when the signal has changed by a factor of $1/e^2$ of the edge height ($\Delta T_{\max}$). For the setup without the MZI, the edge width, τ_1, had a mean value of 341 fs with a standard deviation of 45 fs. For the MZI setup, τ_1 for the intensity had a mean of 311 fs and a standard deviation of 41 fs and, for the phase change, the edge width was 149 fs with a standard deviation of 37 fs. The faster response of the phase with respect to the intensity can be utilized to increase the accuracy of the jitter measurement by using an MZI with the spectral encoding method.

The MZI setup provides a more thorough measurement of the change in the refractive index of the sample. Shown in Fig. 4(e) is a comparison of the arrival time determined by the change in transmission and phase of the optical probe. There is a varying difference between the two, up to 150 fs in some cases, though we expect that this method will be more robust to mechanical instabilities than the standard spectral encoding method, and further testing is required. The unique intensity distribution of each XFEL pulse could be partially responsible for the difference in response time on timescales smaller than the XFEL pulse duration (i.e., 1–10 fs) and is currently under investigation.

Fig. 2. (a) Example of transmitted single shot spectra. The signal (with X-rays), reference (no X-rays), and the relative transmission and corresponding fit are all shown. The black circle indicates the arrival time. (b) Spectra for 2028 single shots ordered by t_0. The black trace indicates the arrival time, t_0. (c) Transmission change with X-ray intensity; the left abscissa shows the number of occurrences in each given X-ray shot energy range. The data points correspond to the right abscissa and show the mean change in sample transmission as a function of shot energy (measured upstream of the Si attenuator by an X-ray gas monitor). The error bars are given as a standard deviation.
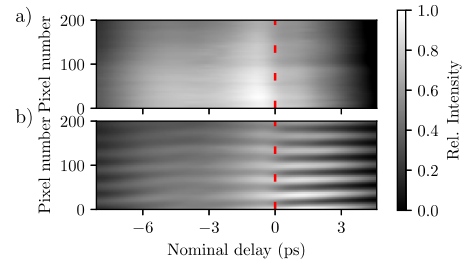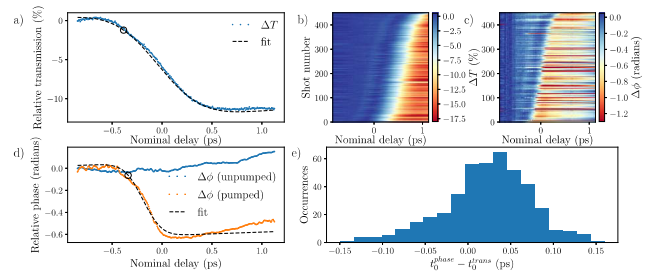

Fig. 4. (a) Relative transmission change for a single shot measured with the MZI setup. The data in (a) and (d) correspond to the same XFEL pulse. The spectra for 450 single shots ordered by time-of-arrival, t_0, using the change in (b) transmission and (c) phase. (d) Phase determined from the interferogram; shown is the phase measured without X-rays and the phase change induced by an XFEL pulse and the corresponding fit. (e) Histogram of the difference in the arrival time determined with both methods. The black circle in (a) and (d) indicates the arrival time, t_0, as determined from the fitting analysis.

This initial jitter measurement with time resolution of 36 fs is not an intrinsic limit and can be improved by increasing the spectrometer magnification and decreasing the temporal chirp of the optical pulse (i.e., shorter pulse duration). Future planned experiments aim to collect higher time resolution data and develop a femtosecond-scale timing tool at the EuXFEL. Stabilization of optical beam transport components and the upgrade from RF to active optical synchronization in the near future is expected to significantly improve the timing jitter.

We have measured the PP timing jitter at the SASE 1 branch of the EuXFEL using the spectral encoding method. The timing jitter was measured to be 308 fs RMS, and with 724 fs FWHM with 36 fs uncertainty, which is comparable to other XFEL facilities using RF synchronization. The jitter between optical and X-ray pulses originates from multiple sources, particularly the 30 m long optical path, vibration in the instruments, temperature, and humidity instability in the SPB/SFX X-ray hutch. Optical synchronization of the PP laser will be available shortly, and the instrument timing jitter will be re-evaluated using the methods described in this Letter. Similarly, other potential jitter sources will be investigated. Future work will explore the timing jitter using multiple pulses per train and the development of a megahertz timing tool. We demonstrated that the detrimental effects of timing jitter at the EuXFEL can be mitigated by using a "measure and sort" approach. We further demonstrated how incorporating an MZI within the spectral encoding setup can be used to determine the change in the complex refractive index of a sample induced by an XFEL pulse on femtosecond timescales. This provides a complementary way to measure the relative delay time by simultaneously measuring the change in the amplitude and phase of the optical probe. This method also provides more flexibility in terms of sample choice, as now the complete change in the complex refractive index can be determined without needing a reference measurement. In principle, a material could be selected where two different properties of each XFEL shot are encoded in the phase and amplitude such as time of arrival and intensity distribution. With higher magnification and, by using a shorter time-of-arrival window, femtosecond-scale timing monitoring will be possible and provided for future experiments as a timing correction tool. We also expect this method to provide useful validation for theoretical studies of the response of materials to XFEL pulses using the known amplitude and phase information.

REFERENCES

1. A. Hosseinizadeh, G. Mashayekhi, J. Copperman, P. Schwander, A. Dashti, R. Sepehr, R. Fung, M. Schmidt, C. H. Yoon, B. G. Hogue, G. J. Williams, A. Aquila, and A. Ourmazd, Nat. Methods **14**, 877 (2017).
2. R. P. Kurta, et al., Phys. Rev. Lett. **119**, 158102 (2017).
3. M. F. Hantke, et al., Nat. Photonics **8**, 943 (2014).
4. H. N. Chapman, et al., Nature **470**, 73 (2011).
5. M. Suga, F. Akita, K. Hirata, G. Ueno, H. Murakami, Y. Nakajima, T. Shimizu, K. Yamashita, M. Yamamoto, H. Ago, and J. R. Shen, Nature **517**, 99 (2015).
6. M. L. Grünbein, et al., Nat. Commun. **9**, 3487 (2018).
7. M. O. Wiedorn, et al., Nat. Commun. **9**, 4025 (2018).
8. T. R. Barends, L. Foucar, A. Ardevol, K. Nass, A. Aquila, S. Botha, R. B. Doak, K. Falahati, E. Hartmann, M. Hilpert, M. Heinz, M. C. Hoffmann, J. Köfinger, J. E. Koglin, G. Kovacsova, M. Liang, D. Milathianaki, H. T. Lemke, J. Reinstein, C. M. Roome, R. L. Shoeman, G. J. Williams, I. Burghardt, G. Hummer, S. Boutet, and I. Schlichting, Science **350**, 445 (2015).
9. K. H. Kim, J. G. Kim, S. Nozawa, T. Sato, K. Young Oang, T. W. Kim, H. Ki, J. Jo, S. Park, C. Song, T. Sato, K. Ogawa, T. Togashi, K. Tono, M. Yabashi, T. Ishikawa, J. Kim, R. Ryoo, J. Kim, H. Ihee, and S. Adachi, Nature **518**, 385 (2015).
10. N. Coquelle, et al., Nat. Chem. **10**, 31 (2018).
11. M. Levantino, B. A. Yorke, D. C. Monteiro, M. Cammarata, and A. R. Pearson, Curr. Opin. Struct. Biol. **35**, 41 (2015).
12. C. Kupitz, et al., Nature **513**, 261 (2014).
13. K. Pande, et al., Science **352**, 725 (2016).
14. P. Nogly, et al., Science **361**, 0094 (2018).
15. P. Emma, et al., Nat. Photonics **4**, 641 (2010).
16. T. Ishikawa, et al., Nat. Photonics **6**, 540 (2012).
17. J. M. Glownia, et al., Opt. Express **18**, 17620 (2010).
18. T. Katayama, S. Owada, T. Togashi, K. Ogawa, P. Karvinen, I. Vartiainen, A. Eronen, C. David, T. Sato, K. Nakajima, Y. Joti, H. Yumoto, H. Ohashi, and M. Yabashi, Struct. Dyn. **3**, 034301 (2016).
19. H.-S. Kang, et al., Nat. Photonics **11**, 708 (2017).
20. E. Saldin, E. Schneidmiller, Y. Shvyd'ko, and M. Yurkov, Nucl. Instrum. Methods Phys. Res., Sect. A **475**, 357 (2001).
21. E. L. Saldin, E. A. Schneidmiller, and M. V. Yurkov, New J. Phys. **12**, 035010 (2010).
22. A. L. Cavalieri, et al., Phys. Rev. Lett. **94**, 114801 (2005).
23. J. Liu, J. Buck, F. Dietrich, W. Freund, J. Grünert, and M. Meyer, "X-ray photon temporal diagnostics for the European XFEL," PUBDB-2014-03618 (2014).
24. J. Liu, F. Dietrich, and J. Grünert, "Technical design report: photon arrival time monitor (PAM) at the European XFEL," XFEL.EU TR-2017-002 (2017).
25. M. Xin, K. Şafak, and F. X. Kärtner, Optica **5**, 1564 (2018).
26. M. R. Bionta, H. T. Lemke, J. P. Cryan, J. M. Glownia, C. Bostedt, M. Cammarata, J. C. Castagna, Y. Ding, D. M. Fritz, A. R. Fry, J. Krzywinski, M. Messerschmidt, S. Schorb, M. L. Swiggers, and R. N. Coffee, Opt. Express **19**, 21855 (2011).
27. F. Tavella, N. Stojanovic, G. Geloni, and M. Gensch, Nat. Photonics **5**, 162 (2011).
28. C. Gahl, A. Azima, M. Beye, M. Deppe, K. Döbrich, U. Hasslinger, F. Hennies, A. Melnikov, M. Nagasono, A. Pietzsch, M. Wolf, W. Wurth, and A. Föhlisch, Nat. Photonics **2**, 165 (2008).
29. D. M. Fritz, et al., Science **315**, 633 (2007).
30. N. Hartmann, W. Helml, A. Galler, M. R. Bionta, J. Grünert, S. L. Molodtsov, K. R. Ferguson, S. Schorb, M. L. Swiggers, S. Carron, C. Bostedt, J.-C. Castagna, J. Bozek, J. M. Glownia, D. J. Kane, A. R. Fry, W. E. White, C. P. Hauri, T. Feurer, and R. N. Coffee, Nat. Photonics **8**, 706 (2014).
31. T. Tschentscher, C. Bressler, J. Grünert, A. Madsen, A. Mancuso, M. Meyer, A. Scherz, H. Sinn, and U. Zastrau, Appl. Sci. **7**, 592 (2017).
32. M. Harmand, R. Coffee, M. R. Bionta, M. Chollet, D. French, D. Zhu, D. Fritz, H. Lemke, N. Medvedev, B. Ziaja, S. Toleikis, and M. Cammarata, Nat. Photonics **7**, 215 (2013).
33. J.-P. Geindre, P. Audebert, S. Rebibo, and J.-C. Gauthier, Opt. Lett. **26**, 1612 (2001).
34. A. P. Mancuso, et al., J. Synch. Rad.(to be published).
35. M. Pergament, G. Palmer, M. Kellert, K. Kruse, J. Wang, L. Wissmann, U. Wegner, M. Emons, D. Kane, G. Priebe, S. Venkatesan, T. Jezynski, F. Pallas, and M. J. Lederer, Opt. Express **24**, 29349 (2016).
36. J. Müller, et al., in Linear Accelerator Conference (LINAC) (MOPO121) (2018), Vol. **113**, pp. 114102.